Available online at www.sciencedirect.com

ScienceDirect

Proceedings of the Combustion Institute 36 (2017) 2927–2935

Proceedings of the Combustion Institute

www.elsevier.com/locate/proci

Regimes describing shock boundary layer interaction and ignition in shock tubes

Kevin P. Grogan, Matthias Ihme*

Department of Mechanical Engineering, Stanford University, Stanford, CA 94305, United States

Received 4 December 2015; accepted 10 June 2016
Available online 12 July 2016

Abstract

Regimes of shock boundary layer interaction are proposed in consideration of shock tube kinetic experiments. For this, we examine three ways that the reflected shock wave interacts with the boundary layer: incipient separation occurs when the shock is just strong enough to subject the flow to an adverse pressure gradient leading to flow reversal; shear layer instabilities manifest after a certain length of time and can cause inhomogeneities in the test gas; and shock bifurcation occurs when the back pressure of the test gas is sufficient to contain the boundary layer fluid within a stagnation bubble causing severe inhomogeneities in the test gas. Theory delineating these regimes is developed, and these delineations are compared to simulations of shock tube experiments as well as experimental data, where reasonable agreement is found. Through the theory applied to the incipient separation regime, it is determined that boundary layer separation likely occurs in most shock tube experiments; however, separation is unlikely to affect a chemical kinetic experiment except at long test times. To quantify the effect of the boundary layer, a bifurcation Damköhler number is introduced, which is found to perform sensibly well at classifying strong and weak ignition in shock tubes, implying that these combustion phenomena are determined by a competition of physical and chemical timescales. Finally, simulations suggest that tailoring the incident shock Mach number for a given experiment could provide opportunities for mitigating inhomogeneities in the test gas.

Keywords: Shock tube; Weak ignition; Shock wave bifurcation; Instabilities; Shock boundary layer interaction

1. Introduction

Shock tubes are a primary tool for chemical kinetic measurements, providing ignition delay times, species time-histories, and elementary reaction rates [1]. They replicate constant-volume reactors to high accuracy for test times up to the millisecond range allowing for idealized zero-dimensional modeling of the combustion process. Furthermore, the test temperature is well-defined as inferred from the speed of the incident shock. An $x - t$ diagram illustrating relevant regions in a shock tube experiment is shown in Fig. 1.

The ideal combustion mode for shock tube experiments is strong ignition, which is characterized

* Corresponding author. Fax: +1 650 725 3525.
E-mail addresses: kgrogan@stanford.edu (K.P. Grogan), mihme@stanford.edu (M. Ihme).

http://dx.doi.org/10.1016/j.proci.2016.06.078
1540-7489

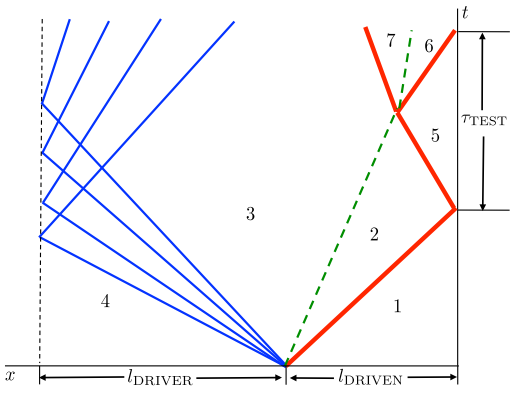

Fig. 1. Diagram illustrating a typical shock tube experiment. Regions are labeled in accordance with standard convention [2]. Shock waves are shown by solid red lines, the contact surface is depicted with dashed green lines, and the expansion fan is represented by thin blue lines. (For interpretation of the references to color in this figure legend, the reader is referred to the web version of this article.)

by the uniform ignition of the test gas at the end wall. However, inhomogeneous or weak ignition has been found in shock tube experiments under certain conditions; weak ignition can occur when pockets of explosive gas ignite prior to the bulk gas. Voevodsky and Soloukhin [3] first studied weak ignition in shock tubes for stoichiometric H_2/O_2 mixtures and showed correlation of the weak-to-strong transition with the second explosion limit of the mixture. Subsequently, Oppenheim and coworkers [4,5] found correspondence with the weak-to-strong transition boundary with an isopleth of the partial derivative of ignition delay with respect to temperature (i.e., $\partial\tau_{ign}/\partial T_5\big|_{p_5} = \text{constant}$), implying that weak ignition results from gas dynamic fluctuations in the test mixture. Yamashita et al. [6] investigated stoichiometric acetylene mixtures and found a correspondence between the origin of ignition kernels and the height of a bifurcating shock wave. Shock wave bifurcation refers to the formation of a λ-shock under certain critical conditions that will be discussed in more detail in Section 2.3. Additionally, reacting simulations of weak ignition in stoichiometric H_2/O_2 mixtures showed that hydrodynamic instabilities resulting from the slip line in a bifurcating shock wave are the primary mechanism for the development of ignition kernels in a shock tube [7,8].

There has been increased interest in recent years for chemical kinetics measurements in shock tubes within the negative temperature coefficient (NTC) region due to advancements in extending shock tube test times [1,9]. However, boundary layer effects can influence the ignition properties for fuels exhibiting NTC characteristics due to an increased sensitivity to the cooler near-wall test gas. Hence, the regimes of interaction of the shock wave with the boundary layer must be understood in order to circumvent inhomogeneous ignition. Therefore, the objectives of this work are to identify the shock boundary layer interaction (SBLI) regimes theoretically, confirm the existence of these regimes through simulations, develop a strategy to ameliorate SBLI, and develop a SBLI regime diagram.

The remainder of this paper proceeds with an analysis of the proposed regimes of SBLI in Section 2, isolating the relevant timescales of the physical processes. This is followed by a description of the mathematical model used for simulations of the SBLI in Section 3. Next, the paper discusses the regimes of SBLI and their occurrence in the simulations in Section 4. Finally, a comparison of the simulations and experimental data against the proposed regimes are presented in Section 5.

2. Shock boundary layer interaction

The interaction of a stationary shock wave with an incoming boundary layer is a well-studied phenomenon [10]. However, the interaction of the reflected shock wave with the incident boundary layer in a shock tube experiment primarily differs from canonical configurations in that the process is fundamentally unsteady; as the reflected shock propagates, it encounters a thickening boundary layer, which alters the character of the interaction. Hence, this gives rise to certain timescales that demarcate regimes where certain effects of the SBLI are introduced or become prevalent. The remainder of this section presents three regimes of SBLI (i.e., incipient separation, shear layer instability, and shock bifurcation) with a focus on the relevant timescales of these regimes.

2.1. Incipient separation

Incipient separation occurs when the adverse pressure gradient imposed by the reflected shock is just sufficient to induce flow separation; this condition is illustrated in the frame of the reflected shock in Fig. 2(a). As depicted in this figure, the boundary layer encounters the reflected shock wave and is either shocked in the supersonic outer layer, decelerated through Mach compression waves in an inviscid inner layer, or passed through a sublayer dominated by viscous effects near the wall. Due to the inability of the fluid to slip at the wall, the shock wave is unable to extend fully to this boundary. Hence, the shock spreads out as a series of compression waves, which brings the boundary layer gas in the inviscid region to the test pressure, p_5. Since the reflected shock wave encounters a boundary layer of weakening attachment to the wall as the shock propagates, there exist a certain time, τ_{IS},

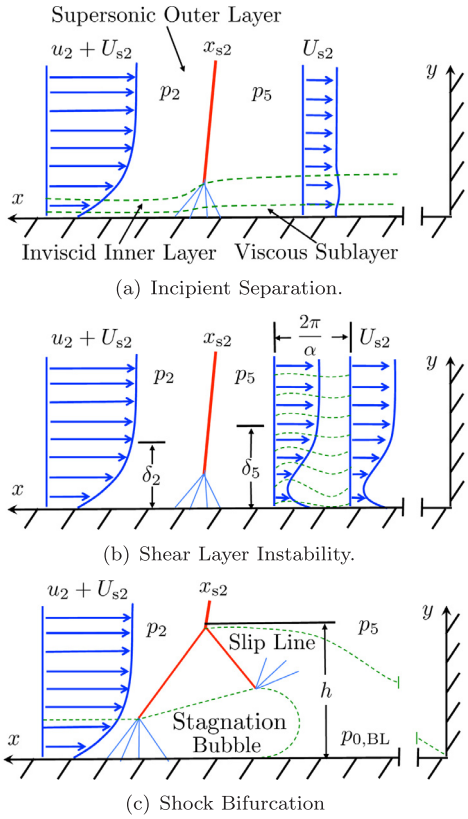

Fig. 2. Illustrations of the postulated SBLI regimes in shock tube experiments. Velocities are given in the frame of the reflected shock.

at which the reflected shock wave overcomes the fluid's attachment to the wall and reverses the flow.

Chapman et al. [11] proposed that the compression in the inviscid layer is akin to a Prandtl–Meyer compression process that adjusts to the displacement of the boundary layer. Additionally, it was recognized that the scaling of the viscous layer at the wall is dependent on the pressure gradient of the free-stream; from these considerations, the following relationship was proposed [11]:

$$\frac{p(x_{s2}-x)-p_2}{\rho_2(U_{s2}+u_2)^2} = \frac{(2C_f)^{1/2}}{\left(M_{s2}^2-1\right)^{1/4}}\mathcal{F}\left(\frac{x_{s2}-x}{l_{IS}}\right), \quad (1)$$

where x_{s2} is the location of the reflected shock, U_{s2} is the speed of the reflected shock, u_2 is the velocity of the gas in region 2 in the laboratory frame, M_{s2} is the Mach number of the reflected shock, $\mathcal{F}(\xi)$ is a universal function with argument ξ, and the incipient separation lengthscale is denoted by l_{IS}. The coefficient of friction, C_f, is evaluated at the location where the boundary layer encounters the shock wave and is found from the similarity solution of Mirels [12].

Incipient separation was found to correspond well to a value of the universal function $\mathcal{F}_{CRIT} = 4.22$ [13]; for this case, the pressure at the separation point is taken to be p_5. Additionally, the skin friction coefficient is related to the incipient separation timescale by $C_f^{-2} \propto x_{s2} + x_{s1} = \tau_{IS}(U_{s2} + U_{s1})$, where x_{s1} indicates the distance that the incident shock would have traveled beyond the end wall if it did not reflect. Using this relation, Eq. (1) can be rewritten as

$$\tau_{IS} = \frac{4C_f^2}{M_{s2}^2-1}\left(\frac{x_{s2}+x_{s1}}{U_{s2}+U_{s1}}\right)\left[\frac{\rho_2(U_{s2}+u_2)^2}{p_5-p_2}\mathcal{F}_{CRIT}\right]^4, \quad (2)$$

where the thermodynamic variables and velocities are known as a function of the incident shock Mach number, M_{s1}, and the specific heat ratio, γ, through normal shock relations [2].

2.2. Shear layer instability

When the reflected shock wave is sufficiently strong, the flow reverses direction in the laboratory frame, and a separated shear layer forms. An illustration of this process is shown in Fig. 2(b). After a certain timescale, instabilities in the shear layer become non-linear, and cool boundary layer fluid mixes with the test gas. This effect would not be conducive to shock tube experiments as it increases the inhomogeneity in the test gas's core region and can create cold-spots; it is proposed that these cold-spots could ignite before the bulk gas. Hence, a characteristic timescale for the boundary layer instability, τ_{INST}, is estimated using the lengthscales and timescales of the linear instability as well as physical dimensions of the boundary layer.

A metric for the inhomogeneity in the test gas is postulated to be V_{BL}/V, where V_{BL} is the volume of the fluid mixed into the test gas from the boundary layer, and V is the total volume of fluid behind the reflected shock at a given time; the total volume is related to the instability timescale by $V \sim \tau_{INST} U_{s2} D^2$. The volume of the mixed boundary layer fluid is found from the characteristic lengthscale of the instability and an estimated characteristic rate at which non-linear vortices form: $V_{BL} \sim V_{VORT} f_{VORT} \tau_{INST}$, where f_{VORT} is the vortex formation frequency. The volume of the vortex should scale with the wavenumber of the most unstable mode of the separated shear layer, α, and the diameter, D, yielding $V_{VORT} \sim D/\alpha^2$. Similarly, the growth rate of the most unstable mode, ω, of the separated shear layer is considered to be related to the formation frequency by $f_{VORT} \sim \omega$. Hence, the ratio of the volume of mixed boundary layer fluid to that of the test gas is given by

$$\frac{V_{BL}}{V} = \beta^{-1/2}\frac{\omega}{U_{s2}D\alpha^2}, \quad (3)$$

where β is some constant. Furthermore, suggesting that $\alpha^{-2} \sim \delta_2^2$ and $\omega^{-1} \propto \delta_2$, the instability timescale may be extricated from Eq. (3) by noting the scaling $\delta_2^2 \sim x_{s2} + x_{s1} = \tau_{INST}(U_{s2} + U_{s1})$:

$$\tau_{INST} = \beta\left[\left(\frac{V_{BL}}{V}\right)_{CRIT}\left(\frac{U_{s2}D\alpha^2}{\omega}\right)\right]^2\left(\frac{x_{s2}+x_{s1}}{U_{s2}+U_{s1}}\right), \tag{4}$$

where $(V_{BL}/V)_{CRIT}$ is a critical ratio of boundary layer fluid to test gas such that the inhomogeneity becomes an appreciable effect; hence, it is postulated that below a critical mixing ratio, the number of discrete pockets of boundary layer fluid are insufficient to yield a probable preignition.

2.3. Shock bifurcation

In the bifurcating shock regime, the reflected shock wave is sufficiently strong such that the back pressure, p_5, is greater than the stagnation pressure of the boundary layer, $p_{0,BL}$. A schematic of the shock bifurcation is shown in Fig. 2(c). A stagnation bubble forms behind the shock and increases in size in an approximately linear fashion in time [14]. A hydrodynamically unstable slip line extends from the triple shock point and is a source of inhomogeneity in the test section. However, shock bifurcation is not a sufficient condition for weak ignition, and the relevant timescales for the bifurcating shock regime must be considered. It is reasonable to assume that weak ignition will not occur if the ignition delay time is much less than a characteristic timescale for the bifurcation (i.e., $\tau_{IGN} \ll \tau_{BIF}$) since the kinetics of the mixture will be unaffected by the physical processes of the bifurcation. A straightforward characterization of the bifurcation timescale is to consider the time at which the bifurcation height, h, equals half the radius, $D/4$, of the shock tube:

$$\tau_{BIF} = \frac{D}{4U_{s2}h'} . \tag{5}$$

The growth of the bifurcation with respect to the distance from the end wall, h', is assumed to be constant and is taken from the empirical relation of Petersen and Hanson [14]:

$$h' = 0.104\,\mathrm{M}_{s1}^{1.07}\gamma^{-2.66}\left(\frac{W}{W_{O_2}}\right)^{-0.37}, \tag{6}$$

where the constant of the original relation is altered by non-dimensionalizing the molecular weight, W, by that of O_2 and by adjusting for the location of the pressure probe to yield the growth of the bifurcation rather than simply the height at a given location.

The theoretical results that have been developed in this section are subsequently verified through simulations in Section 4 and compared against experimental data in a regime diagram in Section 5.

3. Set-up of the simulations

The theoretical analysis presented in Section 2 is complemented by simulations of SBLI in a shock tube. The flow-field is described by the compressible Navier–Stokes equations:

$$\frac{\partial \mathbf{U}}{\partial t} + \frac{\partial}{\partial x_j}\left(\mathbf{F}_j^c - \mathbf{F}_j^v\right) = 0 , \tag{7}$$

where $\mathbf{U}$ is the state vector, and $\mathbf{F}_j^c$ and $\mathbf{F}_j^v$ are the convective and viscous fluxes, respectively. These vectors have the following definitions:

$$\mathbf{U} = [\rho, \rho u_i, \rho e_t]^T , \tag{8a}$$

$$\mathbf{F}_j^c = [\rho u_j, \rho u_j u_i + p\delta_{ij}, u_j(\rho e_t + p)]^T , \tag{8b}$$

$$\mathbf{F}_j^v = \left[0, \tau_{ij}, u_i\tau_{ij} - q_j, \right]^T , \tag{8c}$$

for $i, j \in \{1, 2, 3\}$. The total internal energy is denoted by $e_t = p/(\gamma - 1) + u_i^2/2$, the viscous stress tensor is given by $\tau = \mu\left[\nabla\mathbf{u} - (\nabla\mathbf{u})^{\mathrm{T}}\right] - [2\mu(\nabla \cdot \mathbf{u})/3]\mathbf{I}$, and the heat flux is assumed to obey Fourier's law: $\mathbf{q} = -k\nabla T$. The ideal gas law is used as the state equation, Sutherland's law is used for the viscosity and thermal conductivity, and the gas is assumed to be calorically perfect. For these simulations, a reaction source term is not considered since the development of the SBLI is unlikely to be significantly affected by the relatively slowly changing composition of the test gas.

In this study, 2D simulations are performed to allow the SBLI to be examined at long timescales necessary for the postulated instability mechanism to manifest; additionally, the 2D simulations are performed parametrically by considering a realistic domain. Also, a 3D simulation is performed to study the effects of turbulence and to examine the statistics of the flow.

The governing equations are solved using a block-structured adaptive mesh refinement (AMR) method, which is implemented in the object-oriented framework AMROC (Adaptive Mesh Refinement in Objective-oriented C++) [15–17]. Both the two-dimensional and three-dimensional cases are solved using three levels of adaptive mesh refinement ensuring that all physical processes in smoothly varying regions are properly resolved. Approximately 80 cells across the boundary layer thickness are used for all cases. The smallest grid size at the finest level of refinement is 12.5 μm which is kept constant for all cases, and the observed SBLI regimes are found to be insensitive to further refinement.

For the 2D simulations, the computational domain consists of a symmetric planar shock tube, having a length of 24 cm, and a height of 3 cm. Each simulation is initialized as a Riemann problem, and the boundary layer is allowed to develop

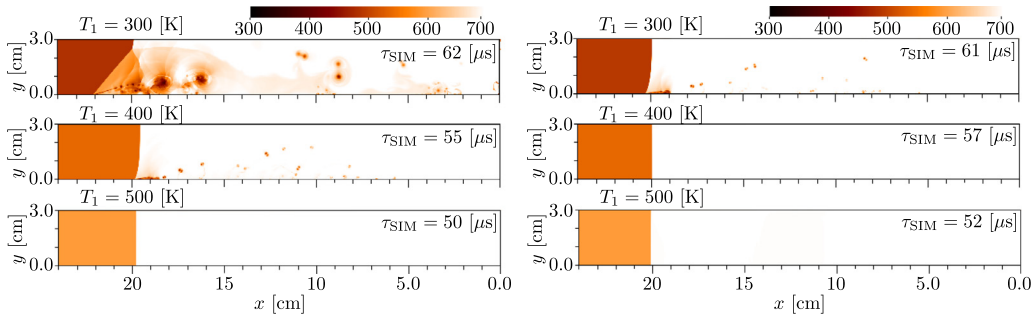

(a) N_2 Dilution. (b) Ar Dilution.

Fig. 3. Comparison of different initial temperatures on the quality of the flow field. Details of the operating conditions of the simulations are presented in Table 1.

behind the shock as it propagates towards and is reflected off the end-wall.

Since the 3D simulation is substantially more demanding computationally than the 2D cases, a reduced domain in a shock-fixed frame is used. The domain consists of a spanwise-periodic planar shock tube, having a length of 30 boundary layer thicknesses, a height of 10 boundary layer thicknesses, and a width of 5 boundary layer thicknesses. The self-similar boundary layer profile of Mirels [12] is injected at the inlet with a thickness of $\delta_{99} = 1$ mm, and outflow boundary conditions are prescribed at the top and end of the domain.

For all simulations, an isothermal, no-slip boundary condition is prescribed at the bottom wall. The wall temperature is set to be approximately room temperature (i.e., 300 K), and for the 3D case, the wall translates at a speed equal to that of the reflected shock in the laboratory frame. The flow-field is initialized by a stationary shock using normal-shock relations [2].

Cases are selected for an inert n-heptane mixture with an equivalence ratio of $\phi = 0.5$, a test temperature of $T_5 = 700$ K, and a test pressure of $p_5 = 2.7$ bar. The matrix of cases for the 2D simulations are presented in Table 1. The cases are selected to span the SBLI regimes, demonstrating the qualitative differences of the SBLI for different diluent gases (i.e., modification of the specific heat ratio), and test gas preheat temperatures (i.e., modification of the incident shock Mach number).

4. Simulation results

4.1. Parametric 2D simulations of n-heptane mixtures

Pseudocolor plots of the temperature field for each simulation listed in Table 1 are shown in Fig. 3. These results demonstrate that for both the nitrogen and argon diluted mixtures, the severity of the SBLI decreases as the initial temperature increases (i.e., as the strength of the incident shock decreases). Nitrogen is shown to yield a much more inhomogeneous flow for comparable conditions than argon. However, the flow becomes quiescent for some initial temperature between 400 K and 500 K. Argon is shown to yield roller vortices that are ingested by the test gas for the 300 K case; however, the flow becomes quiescent at some initial temperature between 300 K to 400 K. Additionally, the nitrogen-diluted cases are shown to span the proposed SBLI regimes with the 500 K, 400 K, and 300 K cases corresponding to Fig. 2(a), (b), and (c), respectively.

The results of these simulations suggest that preheating the mixture may provide a hitherto unconsidered opportunity for reducing some of the inhomogeneities in the flow field by weakening the incident shock wave. Although the feasibility in obtaining a uniformly heated test gas and chemical effects such as fuel pyrolysis may make the application of this strategy challenging, a preheated

Table 1
Summary of the parametric two-dimensional simulations. All mixtures are n-heptane/O_2 with an equivalence ratio of $\phi = 0.5$, a test temperature of $T_5 = 700$ K, a test pressure of $p_5 = 2.7$ bar, and 78.3% diluent of N_2 or Ar. The wall temperature is set to $T_w = 300$ K. The specific heat ratio is evaluated at the test temperature. The abbreviations Dil., Sep., Inst., and Bif. stand for diluent, boundary layer separation, shear layer instability, and shock bifurcation, respectively. A "Y" indicates the occurrence of the effect during the simulation.

ID	Dil.	T_1 [K]	M_{s1}	γ	Sep.	Inst.	Bif.
N2-300	N_2	300	2.05	1.33	Y	Y	Y
N2-400	N_2	400	1.64	1.33	Y	Y	N
N2-500	N_2	500	1.35	1.33	Y	N	N
Ar-300	Ar	300	1.79	1.47	Y	Y	N
Ar-400	Ar	400	1.47	1.47	Y	N	N
Ar-500	Ar	500	1.25	1.47	Y	N	N

Table 2
Summary of the test data in Fig. 6.

Investigators	Mixture	$T_5[K]$	p_5 [bar]	ϕ
Meyer & Oppenheim [4]	H_2/O_2	900–1350	0.2–2	1
Yamashita et al. [6]	C_2H_2/O_2	550–1450	0.5–2	1
Penyazkov et al. [25]	C_3H_8/Air	1000–1750	2–20	0.5, 1, 1.5
Lam et al. [26]	C_3H_8/O_2/Ar	980–1400	6–60	0.5
Pang et al. [27]	H_2/O_2/Ar	908–1118	3–3.7	1

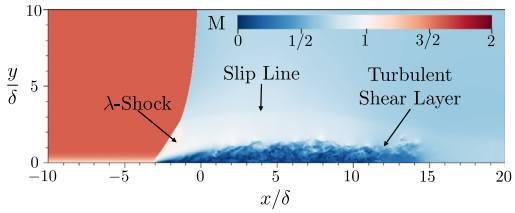

Fig. 4. Snapshot of the 3D simulation colored by Mach number. Interpolated mid-plane data is shown. Results correspond to a test time of $\tau_{TEST} = 1.3$ ms, or spatially, a distance of 42 cm from the end wall. (For interpretation of the color in this figure, the reader is referred to the web version of this article.)

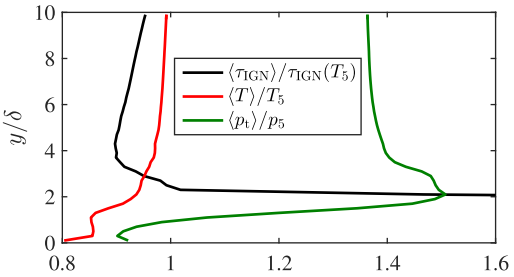

Fig. 5. Profiles for the window $x/\delta \in [5, 10]$. The spatial ignition delay curve is determined from a reduced n-heptane mechanism. (For interpretation of the color in this figure, the reader is referred to the web version of this article.)

test gas could assist in exploring low-temperature autoignition chemistry. Additionally, it is noted that preheating the test gas is utilized in some rapid compression machine and flow reactor experiments [18,19], and preheating has been utilized in shock tubes to prevent fuel condensation [20].

4.2. 3D simulation and evaluation of flow statistics

A pseudocolor plot of Mach number is shown in Fig. 4. The conditions of this 3D simulation correspond to the Ar-300 case listed in Table 2. The equivalent distance of the shock from the end wall (42 cm) is selected to be much larger than the 2D case so that end-wall effects would be negligible. It is postulated that due to the thicker boundary layer in this simulation as compared to the 2D simulation, a λ-shock structure with weak oblique shock waves develops. However, this structure is observed to be static for the duration of the simulation. Hence, the primary characteristic of this regime is the instabilities that manifest from the shock-separated boundary layer, and as shown in the figure, a highly turbulent shear layer near the side wall of the shock tube.

Profiles of normalized temperature, ignition delay, and total pressure for the window of $x/\delta \in [5, 10]$ are shown in Fig. 5. The ignition delay time is taken from an adiabatic, isobaric (HP) reactor using the time at which the concentration of the OH radical has peaked. The chemistry is modeled with a 94-species reduced n-heptane mechanism derived from the detailed mechanism due to Mehl et al. [21] using the procedure of Stagni et al. [22].

The temperature profile is shown to be highly stratified due to the turbulent mixing and the hydrodynamic blockage of the separated boundary layer. Since the temperature increases nearly monotonically with distance from the side wall, the calculated ignition delays demonstrate NTC behavior; at a normalized height of $y/\delta = 4.1$, the ignition delay is shown to be reduced by 10% from the test condition. Hence, it is postulated that the temperature stratification induced by the SBLI is a possible mechanism for near wall preignition.

It is shown that the total pressure of the near wall fluid is less than the test pressure; this suggests that the boundary layer fluid ought to be encapsulated in a stagnation bubble as theorized by Mark [23]. However, since a growing stagnation bubble is not observed in the simulation, it is posited that the turbulent momentum flux of the separated boundary layer balances the pressure gradient.

5. Diagrams of the proposed SBLI regimes

5.1. Examination of the bifurcation timescale and the stagnation pressure ratio

From the ignition delay time and the bifurcation timescale, discussed in Section 2.3, a bifurcation Damköhler number may be formulated as

$$\mathrm{Da}_{\mathrm{BIF}} = \frac{\tau_{\mathrm{BIF}}}{\tau_{\mathrm{IGN}}}. \tag{9}$$

Figure 6 plots the bifurcation Damköhler number against the boundary layer stagnation pressure

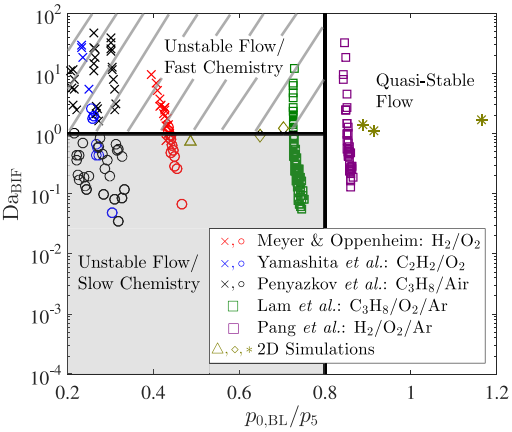

Fig. 6. Diagram of different bifurcation regimes in a shock tube. Particulars of the data are given in Table 2. × indicates observed strong ignition, ○ observed weak ignition, and □ that the quality of the ignition was not reported. For the 2D simulations, * indicates that the flow is found to be quasi-stable, ◇ that the flow shows instability from the separated shear layer, and △ that the simulation shows bifurcation. (For interpretation of the color in this figure, the reader is referred to the web version of this article.)

ratio. The specifics of the test data are given in Table 2, and details of the simulations are given in Table 1. The detailed natural gas mechanism of Petersen et al. [24] is used with an adiabatic, isochoric reactor (UV) model to infer the ignition delays for the data of Meyer and Oppenheim [4], Yamashita et al. [6], and Penyazkov et al. [25]; otherwise, the ignition delays are those reported from the sources. For the simulations, the bifurcation Damköhler number is evaluated to be $\mathrm{Da}_{\mathrm{BIF}} = \tau_{\mathrm{BIF}}/\tau_{\mathrm{SIM}}$.

Three regimes are delineated in Fig. 6: Quasi-Stable Flow, Unstable Flow/Fast Chemistry, and Unstable Flow/Slow Chemistry. The Quasi-Stable Flow regime is delineated using the critical pressure ratio of 0.8 as given by Mark [23]. Experiments in the Quasi-Stable Flow regime have back pressures sufficiently low such that bifurcation is unlikely to occur. The flow is referred to as quasi-stable since there will likely be an unstable separated shear layer within the test time of the experiment; however, the incident shock wave is unlikely to be strong enough to induce instabilities that manifest within the test time. In the Unstable Flow regimes, the back pressure of the test gas is such that bifurcation is likely to develop. Closer to the boundary between the Unstable and Quasi-Stable Flow, 2D simulations show that non-linear instabilities from the separated shear layer manifest; however, strong bifurcation is not shown. This suggest that this line should be treated as a demarcation of where inhomogeneity will likely be injected into the flow by the separated boundary layer, and the distance from this line is indicative of its severity. The correlation of this line to the manifestation of instability is likely due to the similar functional relationship between the pressure ratio and the instability timescale through the incident shock Mach number.

The Unstable Flow/Fast Chemistry and Unstable Flow/Slow Chemistry regimes differ by the bifurcation Damköhler number. As shown in Fig. 6, a bifurcation Damköhler number of unity is found to reasonably classify weak and strong ignition in the test mixtures shown. Hence, above approximately this bifurcation Damköhler number, the chemistry is sufficiently fast such that the gas dynamics of the instabilities and bifurcation are unable to affect the quality of the ignition. However, below this bifurcation Damköhler number, gas dynamics have a significant effect on the chemistry and weak ignition may occur.

The simplicity of the diagram shown in Fig. 6 enables a quick evaluation of the likely test regime of an experiment with respect to shock boundary layer interaction. Hence, the application of such a diagram could be fruitful for shock tube experiments that seek to reduce the dilution of the test gas.

5.2. Comparison of SBLI and chemical timescales

A comparison of the SBLI and chemical timescales is presented in Fig. 7. The simulation timescales, τ_{SIM}, is a reference time for the simulations, taken to be the time at which the reflected shock propagates 20 cm; the snapshots of these cases are shown in Fig. 3. As shown in Fig. 7, the timescale of incipient separation is $\mathcal{O}$(10–100) ns for the Mach numbers shown. This timescale is much faster than the ignition delay at the given Mach number for most chemical kinetic experiments. Hence, it is likely that incipient separation occurs in nearly all shock tube experiments due to the relatively high incident shock Mach number needed to raise the test gas from the ambient temperature to the test temperature.

The instability timescales are found using the same test pressure and diameter as the 2D simulations. From the 2D simulations, the constants in Eq. (4) are determined to be $\beta = 0.05$, and $(V_{\mathrm{BL}}/V)_{\mathrm{CRIT}} = 1 \times 10^{-3}$. With these parameters, reasonable agreement is shown between the observed mixing of boundary layer fluid with the core gas and the theory outlined in Section 2.2 (i.e., the slope of the instability timescale with respect to the Mach number is sufficient to classify the transition between a fast and slow chemistry regime). Hence, the instability of the shear layer is proposed as a plausible source of inhomogeneity in shock tube experiments – one which could potentially lead to weak ignition in the NTC regime.

Preheating the test gas is shown to shift the ignition delay towards a lower Mach number. The

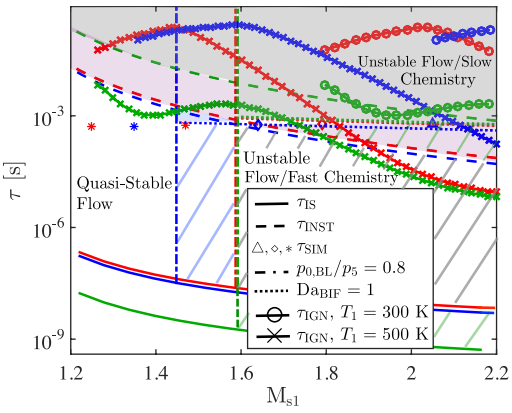

Fig. 7. Comparison of the SBLI and chemical timescales. Test gas is a n-heptane mixture with 78.3% dilution and $\phi = 0.5$. Red denotes argon dilution at 2.7 bar, blue denotes nitrogen dilution at 2.7 bar, and green denotes argon dilution at 27 bar. * indicates that the flow is found to be quasi-stable, $\diamond$ that the flow shows instability from the separated shear layer, and $\triangle$ that the simulation shows bifurcation. The ignition delays, τ_{IGN}, are determined from a reduced n-heptane mechanism created from the procedure outlined in Stagni et al. [22]. The lowest Mach number for each ignition delay curve corresponds to a test temperature of $T_5 = 700$ K. Shading corresponds to the affected mixtures: gray for all mixtures; purple for the low pressure mixtures; blue for the nitrogen diluted mixture: and green for the high pressure mixture. (For interpretation of the references to color in this figure legend, the reader is referred to the web version of this article.)

predominant effect of this is to push ignition delay times past the critical pressure ratio, which allows for more test times in the quasi-stable and fast chemistry regime. Additionally, the lower Mach numbers for the preheated test gases correspond to a higher instability timescale, indicating that less inhomogeneity will likely be in the test gas for a given test temperature as confirmed by simulation.

In addition to preheating the test gas, these results indicate that increasing the test pressure may ameliorate non-ideal gas dynamic effects as well. Specifically, the higher pressure reduces the ignition delay and decreases the inhomogeneities caused by the separated shear layer. The latter is due to the thinner boundary layer at higher pressure, which limits the amount of boundary layer fluid that may be mixed into the test section.

6. Conclusions

The character of the interaction of a reflected shock wave with the boundary layer requires understanding to circumvent inhomogeneous ignition. Through the analysis of three SBLI regimes (i.e., incipient separation, shear layer instability, and shock bifurcation) the following conclusions can be drawn:

1. Boundary layer separation likely occurs in most shock tube experiments; however, there exist a substantial test window before instabilities affect the test gas.
2. Instabilities due to the separated boundary layer can add inhomogeneities to the flow even when the shock wave does not bifurcate.
3. A bifurcation Damköhler number is proposed, which classifies weak and strong ignition in shock tubes for a wide range of mixtures and test facilities reasonably well. This implies that the delineation of strong and weak ignition is a competition of chemical and physical timescales more so than a chemical sensitivity parameter.
4. Simulations show that reducing the Mach number of the incident shock can attenuate the inhomogeneity in the test gas. This is demonstrated through simulations by altering the temperature of the test gas. Additionally, it is observed that increasing the test pressure could mitigate some of the non-ideal gas dynamics.

Hence, different regimes of SBLI can contribute in unique ways to the preignition of a test gas. Additionally, dust particles or fragments from the ruptured diaphragm may contribute to inhomogeneous ignition in the NTC regime; these particles could provide a heat sink for the flow allowing their cooler boundary layer to preignite.

Acknowledgments

The authors gratefully acknowledge financial support through the Air Force Office of Scientific Research under Award No. FA9550-14-1-0219 and the Department of Air Force with Award No. SB20190. The authors would like to thank Dr. Ralf Deiterding for generously allowing us to use his code. Additionally, the authors would like to thank Prof. Ronald Hanson, Dr. David Davidson, and Andrew Tulgestke for several fruitful discussions on shock tube experiments.

References

[1] R.K. Hanson, D.F. Davidson, *Prog. Energy Combust. Sci.* 44 (2014) 103–114.
[2] G. Ben-Dor, O. Igra, T. Elpherin, *Handbook of Shock Waves*, Elsevier, New York, 2001.
[3] V.V. Voevodsky, R.I. Soloukhin, *Proc. Combust. Inst.* 10 (1965) 279–283.
[4] J.W. Meyer, A.K. Oppenheim, *Proc. Combust. Inst.* 13 (1971) 1153–1164.
[5] D.J. Vermeer, J.W. Meyer, A.K. Oppenheim, *Combust. Flame* 18 (1972) 327–336.
[6] H. Yamashita, J. Kasahara, Y. Sugiyama, A. Matsuo, *Combust. Flame* 159 (2012) 2954–2966.

[7] M. Ihme, Y. Sun, R. Deiterding, *AIAA Paper 2013-0538* (2013).
[8] K.P. Grogan, M. Ihme, *Proc. Combust. Inst.* 35 (2) (2015) 2181–2189.
[9] M.F. Campbell, S. Wang, C.S. Goldenstein, et al., *Proc. Combust. Inst.* 35 (2015) 231–239.
[10] D.S. Dolling, *AIAA J.* 39 (8) (2001) 1517–1531.
[11] D.R. Chapman, D.M. Kuehn, H.K. Larson, *Investigation of separated flows in supersonic and subsonic streams with emphasis on the effect of transition, NACA TN 1356*, Ames Aeronautical Lab, Moffett Field, CA, 1958.
[12] H. Mirels, *Laminar boundary layer behind shock advancing into stationary fluid, NACA TN 3401*, Lewis Flight Propulsion Laboratory, Cleveland, OH, 1955.
[13] J. Ostlund, *Flow Processes in Rocket Engine Nozzles with Focus on Flow Separation and Side Loads*, Royal Institute of Technology, 2002 PhD thesis.
[14] E.L. Peterson, R.K. Hanson, *Shock Waves* 15 (2006) 333–340.
[15] R. Deiterding, AMROC - Blockstructured Adaptive Mesh Refinement In Object-oriented C++, 2008. Available at http://amroc.sourceforge.net, last accessed: November 2015.
[16] R. Deiterding, *Comput. Struct.* 87 (2009) 769–783.
[17] R. Deiterding, *J. Combust.* 2011 (738969) (2011) 18 pages.
[18] L. Brett, J. Macnamara, P. Musch, J.M. Simmie, *Combust. Flame* 124 (2001) 326–329.
[19] W.T. Peschke, L.J. Spadaccini, *Report No. EPRI-AP-4291, United Technologies Research Center* (1985).
[20] T. Malewicki, S. Gudiyella, K. Brezinsky, *Combust. Flame* 160 (2013) 17–30.
[21] M. Mehl, W.J. Pitz, C.K. Westbrook, H.J. Curran, *Proc. Combust. Inst.* 33 (2011) 193–200.
[22] A. Stagni, A. Frassoldati, A. Cuoci, T. Faravelli, E. Ranzi, *Combust. Flame* 163 (2016) 382–393.
[23] H. Mark, *J. Aeronaut. Sci.* 24 (1957) 304–306.
[24] E.L. Petersen, D.M. Kalitan, S. Simmons, G. Bourque, H.J. Curran, J.M. Simmie, *Proc. Combust. Inst.* 31 (2007) 447–454.
[25] O.G. Penyazkov, K.A. Ragotner, A.J. Dean, B. Varatharajan, *Proc. Combust. Inst.* 30 (2005) 1941–1947.
[26] K.Y. Lam, Z. Hong, D.F. Davidson, R.K. Hanson, *Proc. Combust. Inst.* 33 (2011) 251–258.
[27] G.A. Pang, D.F. Davidson, R.K. Hanson, *Proc. Combust. Inst.* 32 (2009) 181–188.